On the experimental coupling with continuous interfaces using frequency based substructuring

Domen Ocepek[a], Francesco Trainotti[b], Gregor Čepon[a,*], Daniel J. Rixen[b], Miha Boltežar[a]

[a] *University of Ljubljana, Faculty of Mechanical Engineering, Laboratory for Dynamics of Machines and Structures, Aškerčeva 6, 1000 Ljubljana, Slovenia*
[b] *Technical University of Munich, School of Engineering and Design, Chair of Applied Mechanics, Boltzmannstr. 15, 85748 Garching, Germany*

Abstract

In experimental dynamic substructuring, coupling of substructures sharing a line- or surface-like interface proves to be a challenge due to the difficulties in interface modelling. Modelling a high number of degrees of freedom at the common interface can be too stringent when imposing compatibility and equilibrium conditions, thereby causing redundancy and ill-conditioning. To mitigate the effects of overdetermination and experimental errors, that can lead to a high error amplification, several techniques have been developed, proposing different reduction spaces to weaken the interface conditions. This work investigates reduction space definitions in dynamic substructuring for coupling continuous interfaces. In particular, a comparative investigation of three established techniques, namely the frequency-based modal constraints for fixture and subsystem, singular vector transformation, and virtual point transformation, is conducted within the frequency domain. The feasibility of all approaches is supported by an experimental case study, which can guide practitioners in selecting a suitable approach for their specific needs.

Keywords: Frequency based substructuring, Continuous interface, Modal constraints for fixture and subsystem, Singular vector transformation, Virtual point transformation

1. Introduction

In the field of designing and developing assembled products, a modular approach in the form of substructure-coupling techniques has gained popularity in recent years. Structural dynamic analyses can be carried out more efficiently if the complex assemblies are divided into smaller subsystems. These are then analysed, studied, or optimized separately in the early stage of product design, and later coupled to predict the response model of the final assembly using dynamic substructuring (DS) methods. In a variety of different substructure modelling approaches, numerical and experimental methods are combined and DS can be applied within one of the representative domains [1, 2]. Experimentally obtained response models are usually related to frequency based substructuring (FBS) due to its straightforward implementation with estimated frequency response functions (FRFs).

In the context of experimental FBS, the main challenge for a successful substructure-coupling implementation remains the modelling of the common interface between the substructures [3]. DS requires compatibility of the displacements along the interface between two substructures and the equilibrium of interconnecting forces to be satisfied. Practical difficulties relate to the measurement of an appropriate number of degrees of freedom (DoFs) at which interface conditions are imposed. Coupling too many DoFs can results in redundancy and consequently bad conditioning of the interface coupling equations. Ill-conditioning combined with inevitably present measurement errors (random or systematic in nature) can lead to a high error

*Corresponding author
Email address: gregor.cepon@fs.uni-lj.si (Gregor Čepon)

amplification [4, 5, 6]. Limiting the number of interface measurements and imposing weak compatibility avoids those problems, but can significantly deteriorate the accuracy of the coupled dynamics.

A solution can be applied by projecting the measured dynamics into a representative subspace [1]. This mitigates the effects of measurement errors since the interface conditions are now imposed in the reduced space and are thus related to as weak. Redundant and insignificant dynamic information that is not included in the reduced subspaces is left uncoupled. This is beneficial since this part is commonly strongly affected by measurement errors, is badly controlled or badly observed.

The original virtual point transformation (VPT) [7] uses rigid interface deflection modes (IDMs) to define representative subspace. The method proved to be suitable for point-like interfaces where a relatively small contact area ensures connectivity between the substructures [8]. An extension of the method to include pre-defined flexible IDMs in the reduction bases followed in [9, 10]. The geometrical nature of the transformation enables obtaining the required collocation of the reduced set of DoFs between substructures across the interface although measurements are not performed on matching locations. However, this means the method is sensitive to location bias [11][1].

In the context of component-mode synthesis (CMS), modal constraints for fixture and subsystem (MCFS) [13] is a commonly used approach [14] the use of which was also suggested for FBS in [15]. A flexible fixture is introduced to the coupling workflow and the reduction basis is defined as a truncated set of physical mode shapes of the fixture. Singular vector constraints (SVCs) were introduced in [1] where a reduction basis is defined by dominant singular vectors of the coupled substructure-fixture modal model, obtained by means of singular value decomposition (SVD). In [16], the MCFS is extended by considering the modal bases of both substructures to be coupled when imposing SVCs.

A method developed with the aim to handle flexible interface behaviour in the frequency domain is the singular vector transformation (SVT) [17], where force and displacement reduction spaces are extracted directly from the measured response models by the means of SVD. The method has been proposed in the context of substructure decoupling in [17].

This paper investigates the feasibility of different established approaches to defining a reduction bases for coupling continuous interfaces that resemble line- or surface-like connectivity between the substructures (such as coupling of a gearbox to the engine) and are commonly plagued by difficulties in interface modelling. FBS is selected for comparison due to its versatility in coupling both lightly and/or highly damped structures, establishing its particular advantage in the present context. Thus, an experimental case study is carried out on an assembly of one highly and non-proportionally, and one lightly and proportionally damped substructure. First, a frequency-based MCFS approach is presented that imposes weak interface conditions by using a flexible fixture and its physical mode shapes as a reduction space. Next, the SVT method, which also adopts a fixture in the coupling workflow, is investigated. Lastly, VPT is applied to directly couple two substructures. The benefits, limitations, filtering effect, and conditioning of each approach are investigated in order to provide useful guidelines to the reader for choosing a suitable reduction approach when coupling continuous interfaces.

The paper is organized as follows. In Section 2, a theoretical background on experimental frequency based substructuring is given. Section 3 introduces three strategies to couple continuous interfaces using experimental response models. All presented strategies are then validated in Section 4 on an experimental case study, followed by a short discussion and user-guidelines in Section 5. Finally, conclusions are given in Section 6.

2. Background concepts and notations

This section briefly presents the methodology to couple subsystem admittances when dealing with experimental models. The dual approach to the problem named Lagrange Multiplier - Frequency Based Substructuring (LM-FBS) is presented in Section 2.1, followed by the introduction of weak interface conditions in Section 2.2.

[1] Method's sensitivity to location bias can be significantly reduced using directly measured rotations as shown in [12].

2.1. LM-FBS

The LM-FBS builds the admittance of the assembled system from the admittances of individual subsystems with a set of interface forces as an unknown variable. Consider two substructures A and B assembled at the interface DoFs $(\star)_2^{\mathrm{A}}$ and $(\star)_2^{\mathrm{B}}$, as depicted in Fig. 1.

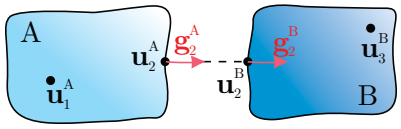

Figure 1: Substructures A and B to be coupled at the common interface.

With admittances of the individual subsystems known ($\mathbf{Y}^{\mathrm{A}}$ and $\mathbf{Y}^{\mathrm{B}}$) and partitioned in internal ($(\star)_1^{\mathrm{A}}$ and $(\star)_3^{\mathrm{B}}$) and interface DoFs, the governing equation of motion for the uncoupled system can be written as[2]:

$$\mathbf{u} = \mathbf{Y}^{\mathrm{A|B}} \left(\mathbf{f} + \mathbf{g} \right),$$

$$\mathbf{u} = \begin{bmatrix} \mathbf{u}_1^{\mathrm{A}} \\ \mathbf{u}_2^{\mathrm{A}} \\ \mathbf{u}_2^{\mathrm{B}} \\ \mathbf{u}_3^{\mathrm{B}} \end{bmatrix}, \quad \mathbf{Y}^{\mathrm{A|B}} = \begin{bmatrix} \mathbf{Y}_{11}^{\mathrm{A}} & \mathbf{Y}_{12}^{\mathrm{A}} & \mathbf{0} & \mathbf{0} \\ \mathbf{Y}_{21}^{\mathrm{A}} & \mathbf{Y}_{22}^{\mathrm{A}} & \mathbf{0} & \mathbf{0} \\ \mathbf{0} & \mathbf{0} & \mathbf{Y}_{22}^{\mathrm{B}} & \mathbf{Y}_{23}^{\mathrm{B}} \\ \mathbf{0} & \mathbf{0} & \mathbf{Y}_{32}^{\mathrm{B}} & \mathbf{Y}_{33}^{\mathrm{B}} \end{bmatrix}, \quad \mathbf{f} = \begin{bmatrix} \mathbf{f}_1^{\mathrm{A}} \\ \mathbf{f}_2^{\mathrm{A}} \\ \mathbf{f}_2^{\mathrm{B}} \\ \mathbf{f}_3^{\mathrm{B}} \end{bmatrix}, \quad \mathbf{g} = \begin{bmatrix} \mathbf{0} \\ \mathbf{g}_2^{\mathrm{A}} \\ \mathbf{g}_2^{\mathrm{B}} \\ \mathbf{0} \end{bmatrix}. \tag{1}$$

The vector $\mathbf{u}$ represents the displacements to the external force vector $\mathbf{f}$, and $\mathbf{g}$ is the vector of interface forces between the substructures that exist only at the interface DoFs, keeping the substructures together.

All subsystems considered are assembled through the proper application of interface conditions. The compatibility of the displacements at the common boundary is recast in the general formulation:

$$\mathbf{B}\,\mathbf{u} = \mathbf{0} \quad \text{where} \quad \mathbf{B} = [\mathbf{0} \quad -\mathbf{I} \quad \mathbf{I} \quad \mathbf{0}]. \tag{2}$$

The equilibrium condition is imposed by replacing the interface forces using a set of unknown Lagrange multiplier vectors $\boldsymbol{\lambda}$ as[3]:

$$\mathbf{g} = -\mathbf{B}^{\mathrm{T}} \boldsymbol{\lambda}. \tag{3}$$

By eliminating the Lagrange multiplier vector from the set of Eqs. (1 - 3) we obtain [1, 2]:

$$\mathbf{u} = \underbrace{\left[\mathbf{I} - \mathbf{Y}^{\mathrm{A|B}} \mathbf{B}^{\mathrm{T}} \left(\mathbf{B}\, \mathbf{Y}^{\mathrm{A|B}} \mathbf{B}^{\mathrm{T}} \right)^{-1} \mathbf{B} \right] \mathbf{Y}^{\mathrm{A|B}}}_{\mathbf{Y}^{\mathrm{AB}}} \mathbf{f}, \tag{4}$$

where $\mathbf{Y}^{\mathrm{AB}}$ is the admittance of the assembled system. Note that different Boolean matrices can be used to apply the compatibility $\mathbf{B}_{\mathrm{u}}$ and equilibrium $\mathbf{B}_{\mathrm{f}}$ conditions (see [8] for more details).

2.2. Interface conditions in the reduced space

The success of Eq. (4) depends strongly on any form of error present while experimentally acquiring subsystems response models (e.g. sensor noise-floor, bias in excitation or response-measurement locations). Directly applying strong compatibility and equilibrium using Eqs. (2) and (3) may lead to unreliable results over the frequency range, especially if the term $\mathbf{B}\,\mathbf{Y}^{\mathrm{A|B}}\,\mathbf{B}^{\mathrm{T}}$ in Eq. (4) is poorly conditioned.

[2] An explicit dependency on the frequency is omitted for the sake of readability. This will be the case for the remainder of the paper.

[3] By choosing interface forces in this form, they are equal in magnitude but act in different directions for any pair of interface DoFs according to Newton's action and reaction principle.

A solution that mitigates the effect of measurement errors can be found by imposing compatibility and equilibrium conditions in a reduced space. Let us apply a reduction matrix $\mathbf{R}_\mathrm{u}$ to the displacement vector $\mathbf{u}$:

$$\mathbf{u} \approx \mathbf{R}_\mathrm{u}\,\mathbf{q} = \begin{bmatrix} \mathbf{I} & & & \\ & \mathbf{R}_\mathrm{u}^\mathrm{A} & & \\ & & \mathbf{R}_\mathrm{u}^\mathrm{B} & \\ & & & \mathbf{I} \end{bmatrix} \begin{bmatrix} \mathbf{u}_1^\mathrm{A} \\ \mathbf{q}_2^\mathrm{A} \\ \mathbf{q}_2^\mathrm{B} \\ \mathbf{u}_3^\mathrm{B} \end{bmatrix}. \tag{5}$$

This projection-based approach can extend the interface to include DoFs that are not strictly located at the physical boundary between A and B (Fig. 2). This is only possible given the collocation of the generalized displacements $\mathbf{q}$ representing the interface displacements in the reduced space is obtained from Eq. (5) (i.e. when $\mathbf{R}_\mathrm{u}^\mathrm{A}$ and $\mathbf{R}_\mathrm{u}^\mathrm{B}$ are partitions from the same physical modes of the interface region). The approach also increases the observability and controllability of the interface dynamics[4]. The generalized displacements are

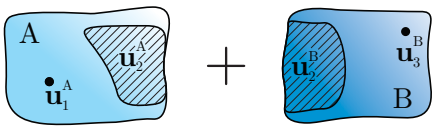

Figure 2: Concept of extended interface, presented as hatched.

computed by pseudo-inversion, denoted with superscript $(\star)^+$:

$$\mathbf{q} = \mathbf{R}_\mathrm{u}^+\mathbf{u} = \mathbf{T}_\mathrm{u}\,\mathbf{u}. \tag{6}$$

The compatibility can now be enforced on collocated DoFs in the reduced space, hence the compatibility condition is weakened:

$$\mathbf{q}_2^\mathrm{B} - \mathbf{q}_2^\mathrm{A} = \mathbf{0} \quad \Rightarrow \quad \mathbf{B}\,\mathbf{q} = \mathbf{B}\,\mathbf{T}_\mathrm{u}\mathbf{u} = \mathbf{0}. \tag{7}$$

Similarly, we apply reduction matrix $\mathbf{R}_\mathrm{f}$ to reduce equilibrium conditions[5]:

$$\mathbf{m} = \mathbf{R}_\mathrm{f}^\mathrm{H}\mathbf{g} = \begin{bmatrix} \mathbf{I} & & & \\ & \left(\mathbf{R}_\mathrm{f}^\mathrm{A}\right)^\mathrm{H} & & \\ & & \left(\mathbf{R}_\mathrm{f}^\mathrm{B}\right)^\mathrm{H} & \\ & & & \mathbf{I} \end{bmatrix} \mathbf{g}, \tag{8}$$

where superscript $(\star)^\mathrm{H}$ denotes a Hermitian (conjugate transpose) operator since, in all generality, the projection space for the forces can be complex. Imposing equilibrium conditions in the reduced space leads to:

$$\mathbf{m} = -\mathbf{B}^\mathrm{T}\boldsymbol{\lambda} \quad \Rightarrow \quad \mathbf{g} = -\mathbf{T}_\mathrm{f}^\mathrm{H}\,\mathbf{B}^\mathrm{T}\,\boldsymbol{\lambda} \quad \text{where} \quad \mathbf{T}_\mathrm{f} = \mathbf{R}_\mathrm{f}^+. \tag{9}$$

By applying weak interface conditions[6] the LM-FBS can be rewritten as follows:

$$\mathbf{u} = \underbrace{\left[\mathbf{I} - \mathbf{Y}^{\mathrm{A}|\mathrm{B}}\,\mathbf{T}_\mathrm{f}^\mathrm{H}\,\mathbf{B}^\mathrm{T}\left(\mathbf{B}\,\mathbf{T}_\mathrm{u}\,\mathbf{Y}^{\mathrm{A}|\mathrm{B}}\,\mathbf{T}_\mathrm{f}^\mathrm{H}\,\mathbf{B}^\mathrm{T}\right)^{-1}\mathbf{B}\,\mathbf{T}_\mathrm{u}\right]\,\mathbf{Y}^{\mathrm{A}|\mathrm{B}}}_{\mathbf{Y}^{\mathrm{AB}}}\,\mathbf{f}. \tag{10}$$

[4] Having a large number of forces and displacements measured in the interface region increases the accuracy in observing and controlling the interface dynamics, thereby improving the accurate evaluation of the interface motion in the chosen representation space $\mathbf{R}_\mathrm{u}$.

[5] The literature usually refers to a weakening of equilibrium when referring to CMS. In cases where incomplete representation bases are used in the modal reduction, this represents dynamics of the substructure in the reduced domain only in the approximate way, thus equilibrium is automatically weakened [1]. In FBS there is no such concept of weakened equilibrium, only weakened compatibility. To fulfill such a weak compatibility only an interface force m in a space of lower dimension is needed.

[6] Although $\mathbf{R}_\mathrm{u}$ and $\mathbf{R}_\mathrm{f}$ do not need to stem from the same interface modes, we assume that force and displacement subspaces have the same dimension (same number of columns in $\mathbf{R}_\mathrm{u}$ and $\mathbf{R}_\mathrm{f}$).

The success of the coupling using Eq. (10) relies on the selection of the reduced subspaces in $\mathbf{R}_\mathrm{u}$ and $\mathbf{R}_\mathrm{f}$ that should include only the dominant dynamic behaviour that is relevant for the assembled configuration.

To summarize, the approach reduces the effect of measurement errors by weakening the interface problem in two manners: the overdetermined nature of Eq. (6) means that only a filtered representation of the interface DoFs is considered for the compatibility, and the underdetermination of Eq. (9) means that interface force distribution is computed to have a minimum W-norm while still having resultant $\mathbf{m}$.

3. Strategies to couple continuous interfaces

Section 2.2 presented general formulation for imposing weak interface conditions to couple the substructures. In the following, three different approaches are applied to the construction of transformation matrices $\mathbf{T}_\mathrm{u}$ and $\mathbf{T}_\mathrm{f}$, namely MCFS, SVT and VPT. Besides the fact that the different approaches rely on different subspaces, they also differ in the coupling workflow. Both MCFS and SVT exploit an additional substructure in the coupling workflow to extend the interface, and measured displacements/forces (referred to as outputs/inputs) must be collocated between substructures across the interface (as explained later). On the other hand, the VPT approach allows the interface to be extended without an additional substructure and also eliminates the requirement for collocation of measured outputs/inputs.

3.1. Modal constraints for fixture and subsystem

A flexible fixture (often named transmission simulator or TS) can be introduced to the coupling workflow and attached to substructure B (see Fig. 3). The combined (sub)structure is denoted as BTS in the following. To enable geometrical collocation for outputs/inputs at the common interface for TS, A and BTS[7], the TS structure should closely resemble the geometry of A to which substructure B will ultimately be connected to[8]. BTS is coupled to the substructure A from which the TS structure is then decoupled to obtain the response model for AB. The procedure is schematically depicted in Fig. 3. Common interface between the substructures is thus extended when compared to the direct coupling (Fig. 1) and includes the full TS substructure where inputs and outputs can be measured at the accessible locations.

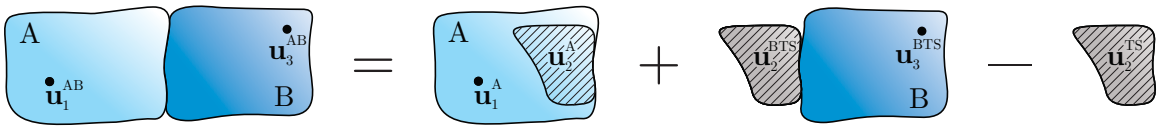

Figure 3: Coupling application with a transmission simulator substructure. Common interface for all substructures is presented as hatched. Note that the transmission simulator is represented only by its interface dynamics since none of its internal DoFs are of interest.

The response of the coupled assembly (with weak interface conditions so that measurement errors do not contaminate the results) now becomes:

$$\mathbf{u} = \underbrace{\left[\mathbf{I} - \mathbf{Y}^{\mathrm{A|BTS|TS}}\,\mathbf{T}_\mathrm{f}^\mathrm{H}\,\mathbf{B}^\mathrm{T}\left(\mathbf{B}\,\mathbf{T}_\mathrm{u}\,\mathbf{Y}^{\mathrm{A|BTS|TS}}\,\mathbf{T}_\mathrm{f}^\mathrm{H}\,\mathbf{B}^\mathrm{T}\right)^{-1}\mathbf{B}\,\mathbf{T}_\mathrm{u}\right]\mathbf{Y}^{\mathrm{A|BTS|TS}}}_{\mathbf{Y}^{\mathrm{AB}}}\,\mathbf{f}, \tag{11}$$

[7] For the sake of convenience, strict geometrical collocation is assumed between the outputs of the substructures involved and, analogously, between the inputs. However, outputs and inputs can be non-collocated between each other, as long as the interface displacements observed from the outputs and the interface forces controlled by the inputs have similar distributions, and all interface DoFs are (implicitly) accounted for.

[8] For further guidelines regarding the design of the TS structure, an interested reader is referred to [1, 13].

where[9]:

$$\mathbf{u} = \begin{bmatrix} \mathbf{u}_1^{\mathrm{A}} \\ \mathbf{u}_2^{\mathrm{A}} \\ \mathbf{u}_2^{\mathrm{BTS}} \\ \mathbf{u}_3^{\mathrm{BTS}} \\ \mathbf{u}_2^{\mathrm{TS}} \end{bmatrix}, \quad \mathbf{Y}^{\mathrm{A|BTS|TS}} = \begin{bmatrix} \mathbf{Y}_{11}^{\mathrm{A}} & \mathbf{Y}_{12}^{\mathrm{A}} & \mathbf{0} & \mathbf{0} & \mathbf{0} \\ \mathbf{Y}_{21}^{\mathrm{A}} & \mathbf{Y}_{22}^{\mathrm{A}} & \mathbf{0} & \mathbf{0} & \mathbf{0} \\ \mathbf{0} & \mathbf{0} & \mathbf{Y}_{22}^{\mathrm{BTS}} & \mathbf{Y}_{23}^{\mathrm{BTS}} & \mathbf{0} \\ \mathbf{0} & \mathbf{0} & \mathbf{Y}_{32}^{\mathrm{BTS}} & \mathbf{Y}_{33}^{\mathrm{BTS}} & \mathbf{0} \\ \mathbf{0} & \mathbf{0} & \mathbf{0} & \mathbf{0} & -\mathbf{Y}_{22}^{\mathrm{TS}} \end{bmatrix}, \quad \mathbf{B} = \begin{bmatrix} \mathbf{0} & -\mathbf{I} & \mathbf{I} & \mathbf{0} & \mathbf{0} \\ \mathbf{0} & \mathbf{0} & -\mathbf{I} & \mathbf{0} & \mathbf{I} \end{bmatrix}. \tag{12}$$

Following the idea of the original MCFS method approach [13], the reduced subspace consists of a truncated set of m TS physical mode shapes. Assume matrix $\mathbf{Y}_{22}^{\mathrm{TS}} \in \mathbb{C}^{N_o \times N_i}$ has at least one input and one output collocated (also known as the driving point). Using multi-reference modal identification, one is able to obtain m mode shapes, each mode shape $r = 1, \ldots, m$ being identified for all output (${}_r\boldsymbol{\phi}_o^{\mathrm{TS}}$) and all input (${}_r\boldsymbol{\phi}_i^{\mathrm{TS}}$) DoFs from the identified modal constant or residue matrix ${}_r\mathbf{A}$ (Fig. 4). For the sake of clarity, subscript $(\star)_2$ is dropped in the following as for the remainder of this section, only interface DoFs are considered unless specified otherwise. Identified input and output modes are then stacked as columns in corresponding mode shape matrices:

$$\boldsymbol{\Phi}_{o,m}^{\mathrm{TS}} = \begin{bmatrix} {}_1\boldsymbol{\phi}_o^{\mathrm{TS}} & {}_2\boldsymbol{\phi}_o^{\mathrm{TS}} & \ldots & {}_m\boldsymbol{\phi}_o^{\mathrm{TS}} \end{bmatrix} \in \mathbb{R}^{N_o \times m}, \quad \boldsymbol{\Phi}_{i,m}^{\mathrm{TS}} = \begin{bmatrix} {}_1\boldsymbol{\phi}_i^{\mathrm{TS}} & {}_2\boldsymbol{\phi}_i^{\mathrm{TS}} & \ldots & {}_m\boldsymbol{\phi}_i^{\mathrm{TS}} \end{bmatrix} \in \mathbb{R}^{N_i \times m}. \tag{13}$$

$${}_r\mathbf{A}^{\mathrm{TS}} = \begin{bmatrix} & & & {}_r\phi_{o_1}^{\mathrm{TS}} \; {}_r\phi_{i_{\mathrm{dp}}}^{\mathrm{TS}} & & \\ & & & {}_r\phi_{o_2}^{\mathrm{TS}} \; {}_r\phi_{i_{\mathrm{dp}}}^{\mathrm{TS}} & & \\ & & & \vdots & & \\ {}_r\phi_{o_{\mathrm{dp}}}^{\mathrm{TS}} \; {}_r\phi_{i_1}^{\mathrm{TS}} & {}_r\phi_{o_{\mathrm{dp}}}^{\mathrm{TS}} \; {}_r\phi_{i_2}^{\mathrm{TS}} & \cdots & {}_r\phi_{o_{\mathrm{dp}}}^{\mathrm{TS}} \; {}_r\phi_{i_{\mathrm{dp}}}^{\mathrm{TS}} & \cdots & {}_r\phi_{o_{\mathrm{dp}}}^{\mathrm{TS}} \; {}_r\phi_{i_{N_i}}^{\mathrm{TS}} \\ & & & \vdots & & \\ & & & {}_r\phi_{o_{N_o}}^{\mathrm{TS}} \; {}_r\phi_{i_{\mathrm{dp}}}^{\mathrm{TS}} & & \end{bmatrix}$$

Figure 4: Extracting r-th TS output (${}_r\boldsymbol{\phi}_o^{\mathrm{TS}}$ -) and input (${}_r\boldsymbol{\phi}_i^{\mathrm{TS}}$ -) modes from the modal constant matrix[10].

The transformation matrices for the MCFS approach in the frequency domain[11] are defined as:

$$\mathbf{T}_{\mathrm{u}} = \begin{bmatrix} \mathbf{I} & & & \\ & \left(\boldsymbol{\Phi}_{o,m}^{\mathrm{TS}}\right)^{+} & & \\ & & \left(\boldsymbol{\Phi}_{o,m}^{\mathrm{TS}}\right)^{+} & \\ & & \mathbf{I} & \\ & & & \left(\boldsymbol{\Phi}_{o,m}^{\mathrm{TS}}\right)^{+} \end{bmatrix} \quad \text{and} \quad \mathbf{T}_{\mathrm{f}} = \begin{bmatrix} \mathbf{I} & & & \\ & \left(\boldsymbol{\Phi}_{i,m}^{\mathrm{TS}}\right)^{+} & & \\ & & \left(\boldsymbol{\Phi}_{i,m}^{\mathrm{TS}}\right)^{+} & \\ & & \mathbf{I} & \\ & & & \left(\boldsymbol{\Phi}_{i,m}^{\mathrm{TS}}\right)^{+} \end{bmatrix} \tag{14}$$

and the assembly is performed using Eq. (11). Using the same reduction basis for interface DoFs from all substructures retains the collocation in the reduced domain given that the measurements on all substructures are performed in a collocated manner. The interface between A and B can actually be continuous given that properly controlled and observed flexible mode shapes are retained in the reduction step.

[9] A decoupling step is denoted with a negative admittance matrix for the subsystem to be disassembled.
[10] The abbreviation dp stands for the driving point where the input and output DoF are collocated.
[11] The interested reader is referred to Appendix A where this reduction is further elaborated.

3.2. Singular vector transformation

Singular vector transformation shares similarities with the MCFS method presented above. Again, the issues with the collocation of measured DoFs at both sides of the interface can be resolved by including the TS substructure in the coupling process. Whereas the MCFS method uses a truncated set of physical TS mode shapes for the weakening step, SVT uses a truncated set of TS singular modes as explained next.

Performing singular value decomposition [18] per frequency line on a TS admittance matrix $\mathbf{Y}^{\mathrm{TS}}$ one obtains:

$$\mathbf{Y}^{\mathrm{TS}} = \mathbf{U}^{\mathrm{TS}} \mathbf{\Sigma}^{\mathrm{TS}} \left(\mathbf{V}^{\mathrm{TS}}\right)^{\mathrm{H}}, \tag{15}$$

where $\mathbf{U}^{\mathrm{TS}}$ and $\mathbf{V}^{\mathrm{TS}}$ are orthonormal matrices of the left- and right singular vectors of $\mathbf{Y}^{\mathrm{TS}}$. $\mathbf{\Sigma}^{\mathrm{TS}}$ is a diagonal matrix of real, non-negative singular values of $\mathbf{Y}^{\mathrm{TS}}$, arranged in descending order. Column vectors of $\mathbf{U}^{\mathrm{TS}}$ and $\mathbf{V}^{\mathrm{TS}}$ can be respectively seen as approximate mode shapes and approximate mode participation factors at individual frequency line with associated singular values indicating the importance of their contribution.

For the reduced subspace, only m most dominant singular modes at each frequency line are retained[12]. The transformation matrices for the SVT approach can thus be expressed as:

$$\mathbf{T}_{\mathrm{u}} = \begin{bmatrix} \mathbf{I} & & & \\ & \left(\mathbf{U}_m^{\mathrm{TS}}\right)^{\mathrm{H}} & & \\ & & \left(\mathbf{U}_m^{\mathrm{TS}}\right)^{\mathrm{H}} & \\ & & & \mathbf{I} \\ & & & & \left(\mathbf{U}_m^{\mathrm{TS}}\right)^{\mathrm{H}} \end{bmatrix} \quad \text{and} \quad \mathbf{T}_{\mathrm{f}} = \begin{bmatrix} \mathbf{I} & & & \\ & \left(\mathbf{V}_m^{\mathrm{TS}}\right)^{\mathrm{H}} & & \\ & & \left(\mathbf{V}_m^{\mathrm{TS}}\right)^{\mathrm{H}} & \\ & & & \mathbf{I} \\ & & & & \left(\mathbf{V}_m^{\mathrm{TS}}\right)^{\mathrm{H}} \end{bmatrix} \tag{16}$$

and the assembly is performed using Eq. (11). In this manner, flexible interface motion (if properly controlled and observed) can be retained in the coupling process. Hence, SVT can be seen as a suitable tool to couple continuous interfaces. Furthermore, frequency dependent bases adjusts for the dominant singular modes based on their contribution (unlike the MCFS method). Using the same reduction bases for all substructures ensures compatibility of interface DoFs in the reduced domain (hence the motivation to adopt the TS substructure in the coupling workflow).

3.3. Virtual point transformation

With virtual point transformation, columns in $\mathbf{R}_{\mathrm{u}}$ and $\mathbf{R}_{\mathrm{f}}$ are selected as interface deflection modes defined by relative measurement location and orientation with respect to the virtual point (VP) [7], chosen near the physical interface (Fig. 5).

The use of geometry dependent reduction bases leads to collocated generalized coordinates (VPs) for both substructures, for which interface conditions are then imposed. This in turn avoids the need for adding an additional flexible fixture to the coupling process as discussed above, significantly reducing measurement effort. The coupled response is obtained using Eq. (4).

Commonly, a reduction using a geometrical basis is performed by means of rigid IDMs only. That means the interface flexibility is left uncoupled, posing an issue for coupling continuous interfaces and thus limiting the approach for interfaces that only behave rigidly. In order to overcome this issue, two methodologies may be adopted:

- Use of additional non-collocated virtual points that can approximate flexible interface motion by piecewise rigid interface regions and hence implicitly account for flexible interface DoFs.
- Including flexible IDMs in the defined reduction bases $\mathbf{R}_{\mathrm{u}}$ and $\mathbf{R}_{\mathrm{f}}$ that are defined from the relative location of the measurement position with respect to the virtual point [9, 10]. However, the manual selection of flexible IDMs included in the reduction spaces is a case-specific cumbersome task that often relies on user-judgment.

[12] The selection of m is left to the user and can be facilitated by a graphical presentation of singular values with respect to the frequency, see for instance Complex Mode Indicator Function (CMIF) [19].

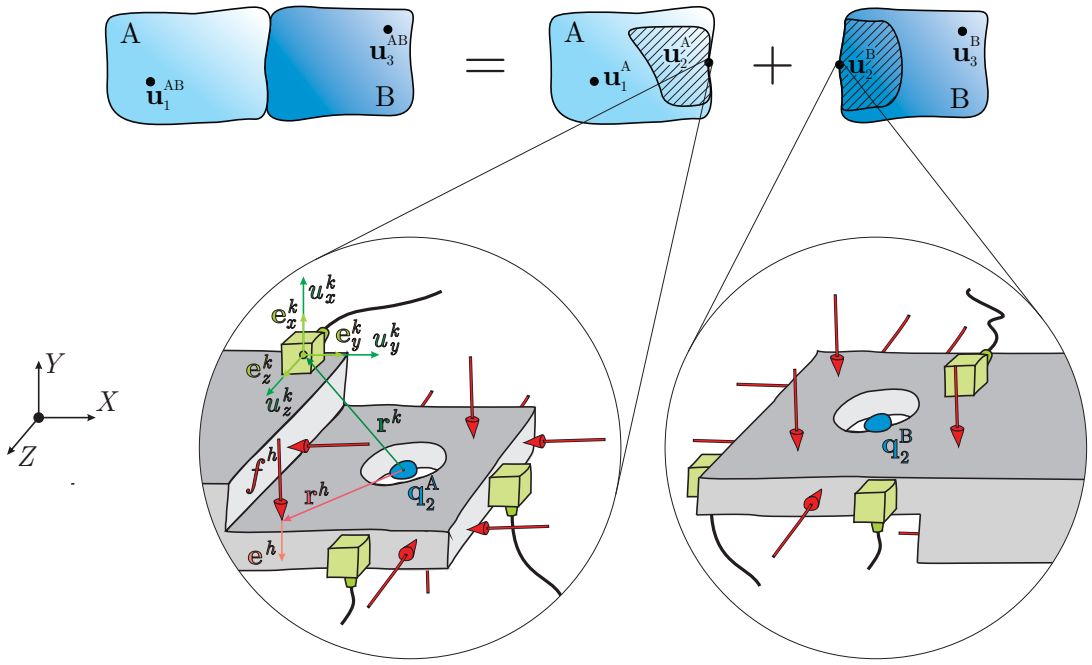

Figure 5: Coupling application with a virtual point[13]. Note that measured outputs and inputs on individual substructures are not required to be collocated, just the virtual points.

Note that all approaches require considerable measurement effort in order to ensure sufficient over/under-determination of the output/input transformations. Furthermore, all approaches are sensitive to bias errors in input/output position/direction, although this can be identified to some extent by measurement quality indicators [7].

4. Experimental case study

Experimental validation of all three presented approaches was performed within a coupling application of two substructures sharing a common surface-like interface. The experimental setup used is presented in Section 4.1. Considerations on obtaining the transformation matrices are presented in Section 4.2, followed by the coupling results in Section 4.3.

4.1. Experimental setup

An assembly of two aluminium substructures, presented in Fig. 6, is the object of this study[14]. The boundary conditions were applied by fixing the assembly AB (through substructure A) to a vibration-free table using steel cylindrical supports. Contact areas between A and the cylindrical supports were padded with rubber pads that introduced local high damping in the structure and thus motivated the use of frequency based substructuring instead of modal-based coupling approaches for this case (see also discussion in Appendix B). Connectivity with the vibration-free table was ensured by two M10 bolts, top washers and tightening torque of approximately 10 Nm. The connectivity at the interface between A and B was ensured by four M10 bolts with locking nuts, top/bottom washers and a tightening torque of approximately 20 Nm, motivated to minimize the effect of contact flexibility or non-linearities.

[13]The position vector from the VP to the center of the triaxial accelerometer is denoted by $\mathbf{r}^k$. The unit vector for each sensor axis is $\mathbf{e}_i^k$ and the response in each axis is denoted by u_i^k ($i \in (x, y, z)$). The position vector from VP to the force impact is $\mathbf{r}^h$, the impact direction is $\mathbf{e}^h$ and the impact magnitude is f^h.

[14]CAD models for all substructures considered in this study are freely available at the *pyFBS* repository [20].

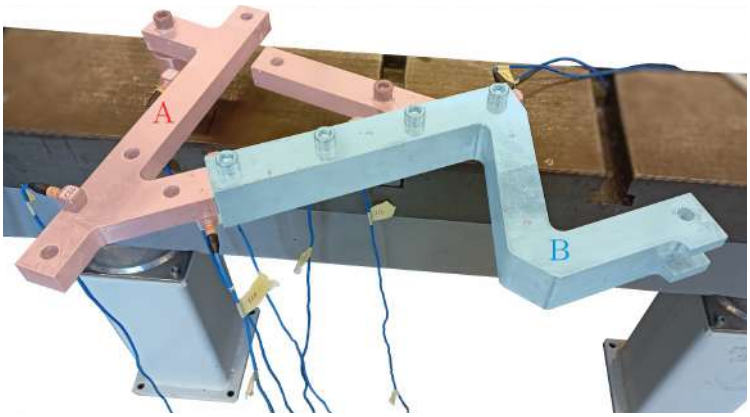

Figure 6: Overview of the assembled system AB.

Eight Kistler 8688A triaxial modal accelerometers were glued to the surface using cyanoacrylate glue. Six of them were homogeneously distributed at the points on A and on TS between which compatibility will be (weakly) enforced, with the other two fixed to the internal DoFs of A away from the interface (Fig. 7a). 26 impacts were performed, with 18 of them homogeneously distributed over the common area of A and TS, and 8 of them at the internal DoFs of B (Fig. 7a). The excitation source was a PCB 086C03 modal hammer equipped with a vinyl tip. The H-1 estimator was chosen for assembling the admittance matrix with six impact repetitions per individual excitation location for all measurement campaigns.

To obtain a response model for substructure A, substructure B was then removed from the assembly (Fig. 8) without changing any boundary or mass loading conditions (coming from sensors fixed to substructure A). FRFs of A were measured for the same 18 impact locations at the A/TS intersection and 24 response locations (18 at the interface and 6 away from the interface, Fig. 7b).

The next measurement campaign comprised the TS substructure. All impact and response locations at the A/TS intersection were carefully moved to the TS, aiming to preserve collocation. The free boundary conditions of TS were approximated by hanging the substructure on thin rubber cords. FRFs of TS were measured for 18 impact and 18 response locations (Fig. 7c).

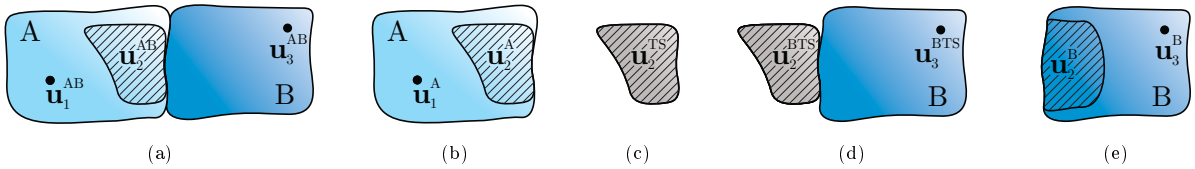

Figure 7: Schematic depiction of all measurements campaign with DoFs to be measured for each system; a) final assembly AB, b) substructure A, c) substructure TS, d) substructure BTS, e) substructure B.

Substructure B was then assembled with TS to form a BTS assembly, keeping the sensors on TS exactly as in the previous step. The connectivity between B and TS was a replica of the one of AB (with four M10 bolts, nuts and washers, tightened together to reach the 20 Nm torque level). Hence the joint between B and TS replicated the actual joint in the assembly AB as closely as possible[15]. The free boundary conditions of BTS were again approximated using thin rubber cords (Fig. 9). In total, FRFs of BTS were measured for all 26 impact and 18 response locations (Fig. 7d).

The final measurements campaign was performed on substructure B. For this, 18 impacts and 6 accelerometers were homogeneously distributed in the vicinity of the common interface between A and B

[15]Because of this, the resulting experimental substructure inherently includes the linearized stiffness and damping in the joint, which coupling workflow A+B usually neglects [1].

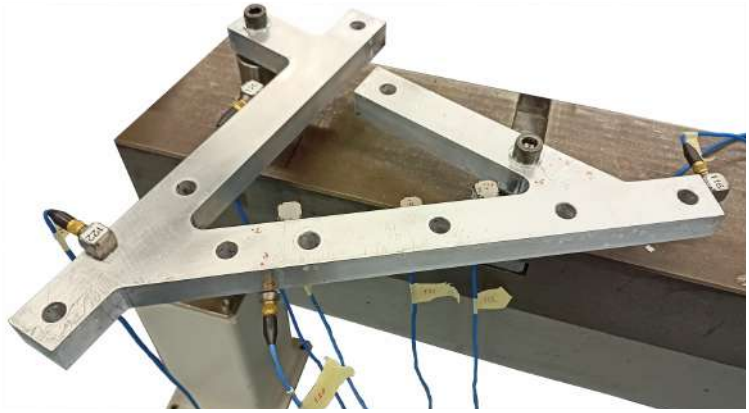

Figure 8: Overview of the substructure A.

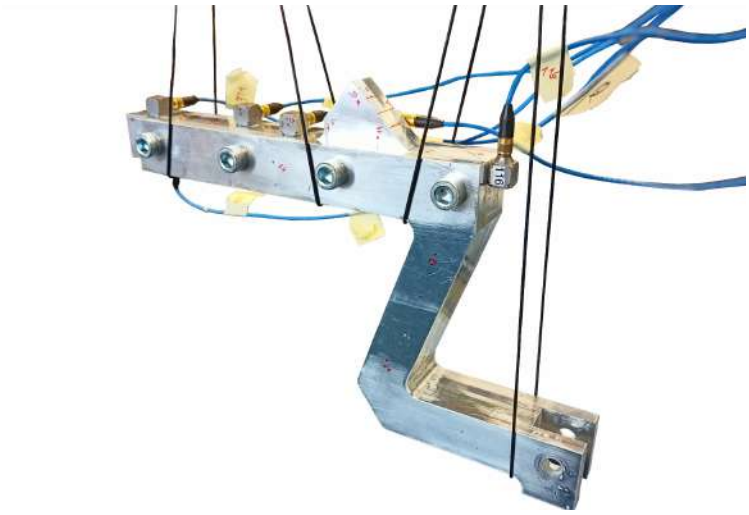

Figure 9: Overview of the assembled system BTS.

(Fig. 7e). 8 impacts at B's internal DoFs were retained, thus FRFs were measured for 26 impact and 18 response locations (Fig. 7e).

4.2. Obtaining the transformation matrices

The coupling approach with the MCFS method adopted the workflow presented in Fig. 10. First, multi-reference modal identification [21] implemented within the *python* package *pyFBS* [20] was used to obtain the first three flexible output and input modes from $\mathbf{Y}^{\mathrm{TS}}$ (see Eq. 13) that were adequately controlled and observed in the TS measurement campaign. Modes were properly mass-normalized[16] by using the driving point information included in the measurements. The flexible modes were then added to the 6 rigid body modes, obtained using a numerical model of TS and stacked into transformation matrices $\mathbf{T}_{\mathrm{u}}$ and $\mathbf{T}_{\mathrm{f}}$ as described in Section 3.1. Finally, the response model for AB was obtained using Eq. (11).

The same workflow in Fig. 10 was then adopted for the SVT approach. Ten dominant singular modes ($m = 10$, based on CMIF plot[17]) of $\mathbf{Y}^{\mathrm{TS}}$ at each frequency line were retained for the reduction bases.

[16] Mass-normalization of modes is not required but performed anyway as the TS substructure is lightly and proportionally damped, thus its modes should be real. Different normalization of modes would only change the projection space.

[17] For the sake of simplicity, a constant number of singular modes was retained for the reduction bases throughout entire frequency range of interest.

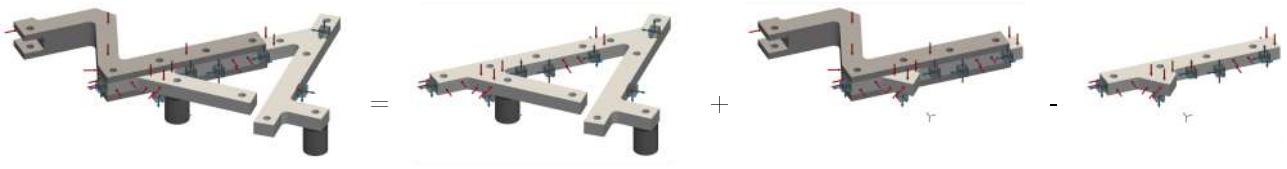

(a) (b) (c) (d)

Figure 10: Coupling workflow using flexible fixture; a) final assembly AB, b) substructure A, c) substructure BTS, d) substructure TS.

Transformation matrices $\mathbf{T}_\mathrm{u}$ and $\mathbf{T}_\mathrm{f}$ (see Eq. 16) were constructed using *pyFBS* and the assembly was performed using Eq. (11).

(a) (b) (c)

Figure 11: Coupling workflow using virtual point transformation; a) final assembly AB, b) substructure A, c) substructure B.

For the VPT approach, two VPs (12 DoFs in total) were defined at arbitrary locations in the proximity of the interface, denoted as green spheres in Fig. 11c. As the interface in this study can be considered as continuous, the use of multiple VPs for coupling was preferred to including flexible IDMs due to the difficulty of selecting a representative extended basis for flexible DoFs. The workflow presented in Fig. 11 consisted of coupling A and B directly without the use of TS. Hence both VPs were collocated at both substructures. For each substructure, 9 impacts and 9 responses in the proximity of the interface were attributed to each individual VP[18]. Based on their relative positions with regards to the VPs, transformation matrices $\mathbf{T}_\mathrm{u}$ and $\mathbf{T}_\mathrm{f}$ were constructed from rigid IDMs using *pyFBS*. Finally, the response model of the assembly was obtained using Eq. (10).

4.3. Results

The final coupling results for all three proposed approaches are presented in Fig. 12 and compared to the reference. Overall, 26×24 reference FRFs were available, yet only one input/output relation is presented here as the findings are analogous for all examined FRFs.

To quantify the agreement between the coupled prediction for each approach and the reference, an amplitude and phase-sensitive coherence criterion [7] is adopted. The criterion is bounded between 0 and 1, with values closer to 1 indicating a strong correlation between the compared responses. In Fig. 13, the coherence for each approach is presented in relation to frequency.

The comparison of the MCFS and SVT approaches indicates that both methods yield similar results across the majority of the examined frequency range. However, SVT slightly outperforms MCFS throughout the entire frequency range of interest (as confirmed by Fig. 13), suggesting that the SV-based selection principle directly from the measurements allows for a properly controlled and observed space to be included in the reduction bases. As MCFS uses a constant subspace for each frequency line, it yields a poor approximation especially at higher frequencies where the modal density becomes higher. Both approaches significantly reduce the effect of noise at higher frequencies. However, this is not that apparent at low

[18] Response channels and impacts attributed to each VP were equally distributed in all directions and did not point straight to the VP in order to observe and control VP's rotational DoFs.

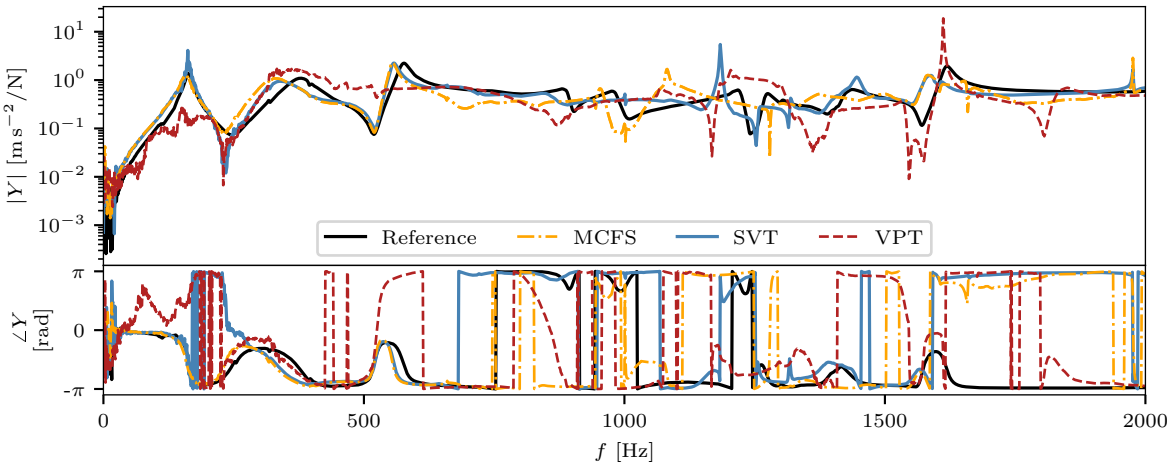

Figure 12: Amplitude and phase of a FRF of $\mathbf{Y}^{\mathrm{AB}}$ using proposed approaches.

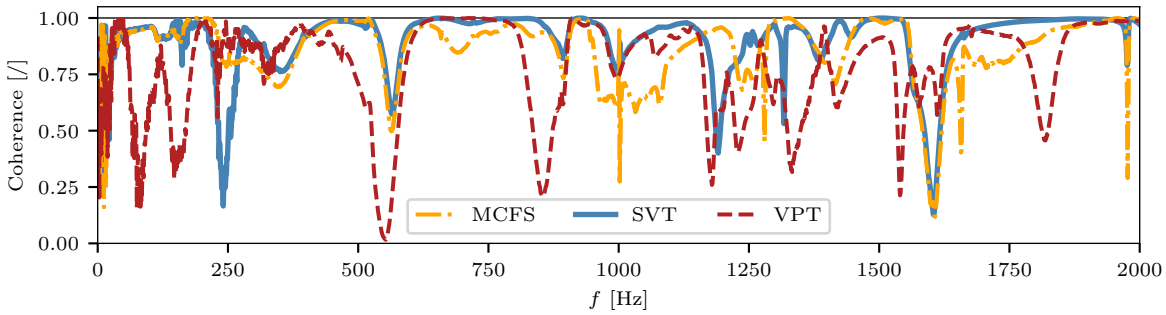

Figure 13: Coherence criterion for each approach and the reference in relation to frequency.

frequencies due to the relatively high number of DoFs retained in the interface modelling [17]. Similarly, for both approaches, some spuriousities are observed, particularly at higher frequencies.

The VPT approach generally leads to a reduced response accuracy with less prominent filtering effect. High amount of noise at lower frequencies is attributed to the high number (12) of VP DoFs which leads to bad conditioning of the interface flexibility matrix (discussed in the following). For this reason truncated SVD (TSVD) [22] was applied to the VP interface flexibility matrix (term $\mathbf{B}\,\mathbf{T}_{\mathrm{u}}\,\mathbf{Y}^{\mathrm{A|B}}\,\mathbf{B}\,\mathbf{T}_{\mathrm{f}}$ in Eq. (10)) by discarding the lowest 1 % of singular values at each frequency line in the inversion. The TSVD-based prediction is presented in Fig. 14 where an improved agreement with the reference is observed. In some frequency bands, TSVD appears to be too severe, leading to spurious dynamics being present in the response.

Some further considerations that can be taken into account when evaluating reduction approaches are addressed next.

4.3.1. Filtering

A quick assessment indicating the adequate selection of the reduction bases can be performed by inspecting filtered FRFs $\widetilde{\mathbf{Y}}$ (projected into reduced space and then back-projected using the selected reduction bases):

$$\widetilde{\mathbf{Y}} = \mathbf{R}_{\mathrm{u}}\,\mathbf{T}_{\mathrm{u}}\,\mathbf{Y}\,\mathbf{T}_{\mathrm{f}}^{\mathrm{H}}\,\mathbf{R}_{\mathrm{f}}^{\mathrm{H}}. \tag{17}$$

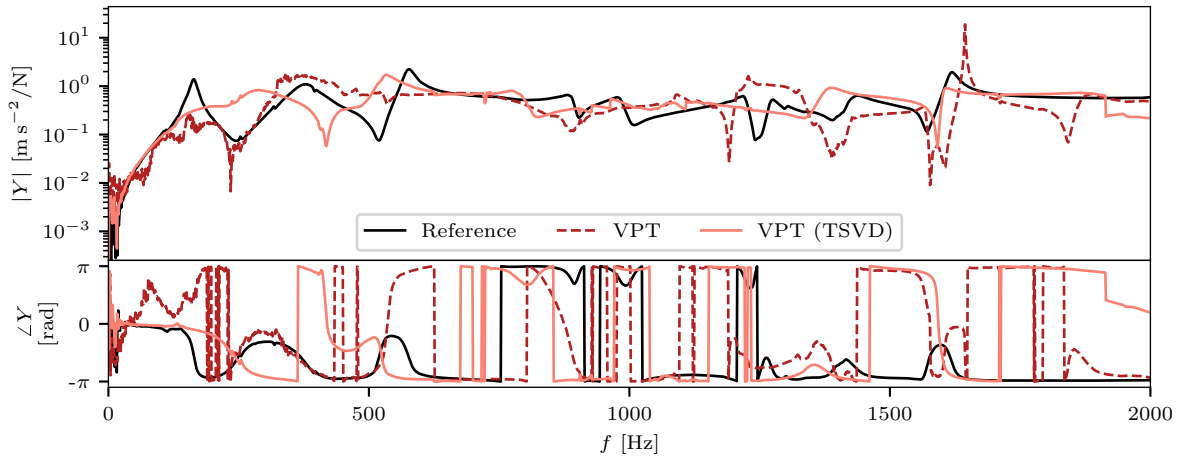

Figure 14: Amplitude and phase of a FRF of $\mathbf{Y}^{\mathrm{AB}}$ using VPT and VPT with singular value truncation.

By visualizing filtered FRFs against the measured ones ($\mathbf{Y}$) for substructure A (Fig. 15), one can determine how selected reduced subspaces represent the dynamics of A. The filtering effect for the MCFS and SVT approach appears to be similar in the low frequency range. Especially for the MCFS approach, filtering is quite severe in the high frequency range (1000 - 2000 Hz), which indicates the need of additional modes in the reduction to improve the coupling prediction as the filtered response is left uncoupled. As expected, due to the high number of DoFs used in the transformation for the VPT approach, the filtering effect is light.

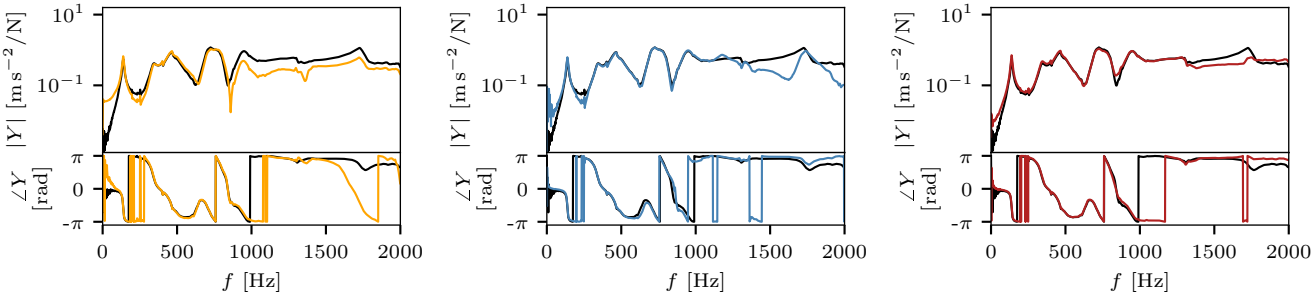

Figure 15: Measured and filtered FRF of $\mathbf{Y}^{\mathrm{A}}$; a) MCFS (— measured, — filtered), b) SVT (— measured, — filtered), c) VPT (— measured, — filtered).

4.3.2. Conditioning

Finally, some remarks are given on the interface flexibility matrix conditioning (Fig. 16), as its high condition number might cause error amplification in the predicted response.

Both MCFS and SVT approaches exhibit similar and fairly low condition number throughout the entire frequency range of interest, meaning the reduction bases are well chosen. This in turn causes efficient error minimization in the reduction step.

The high condition number of the VPT approach is attributed to the presence of redundant (linearly-dependent) DoFs through the whole frequency range, hence the argument to use TSVD in the inversion. Especially as the substructures are very stiff in the direction along the interface, lack of flexible motion makes some DoFs redundant.

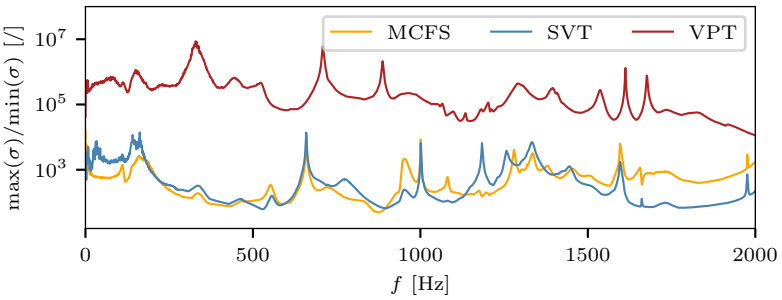

Figure 16: Condition number of the interface flexibility matrix for all studied approaches.

4.3.3. TS as a numerical model

If the basic requirements when designing a TS substructure [13] are met, TS can be accurately modelled numerically with ease. In the following, the use of numerical TS structure is investigated by fully replacing experimental TS response model in the MCFS and SVT approaches.

This is particularly advantageous for the MCFS approach, as a larger number of flexible mode shapes, that are otherwise experimentally unattainable due to the limitations of the measurement equipment, can be used to enrich the reduction bases. Additionally, introduction of numerical TS avoids modal identification step, which might be problematic due to the manual pole selection by the user. With numerical models, each mode will have some (albeit small) contribution at each frequency line which is not the case for experimental models where this contribution cannot always be measured. Thus controllability- and observability-related issues can be avoided, which benefits both MCFS and SVT. Another advantage of using a numerical model for the TS is the reduced measurement effort in the MCFS and SVT coupling workflow.

In Eq. (12), the experimental response model of TS ($\mathbf{Y}_{22}^{\mathrm{TS}}$) was replaced by a numerical one. Numerical physical and singular modes were used in construction of transformation matrices for MCFS (Eq. (14)) and SVT (Eq. (16)) approach, respectively. The results where the number of mode shapes and singular modes retained in the reduction bases varied from 6 to 12 (with a step of 2) are presented in Fig. 17. The performance of both approaches is alike which is additionally confirmed by the coherence criterion. It is evident that the filtering effect of the reduction decreases while enriching the reduction basis with additional modes. Results indicate that both approaches would benefit from frequency dependent reduction bases, as a reasonably higher number of DoFs retained in the reduction improves prediction in a higher frequency range and vice versa (although six physical/singular modes clearly do not form a representative reduction subspace for this specific case study).

5. Discussion

An experimental study presented the feasibility of all three approaches for coupling continuous interfaces. A highly damped assembly was selected to get out of the 'comfort zone' of CMS and demonstrate the versatility and robustness of the FBS[19]. The following observations might help the reader choosing a suitable reduction basis for his/her requirements.

A robust modal identification process is required to obtain flexible modes for the MCFS approach. This process is rarely automated, even for lightly damped systems with well-separated modes, and thus requires a selection based on user judgment. The MCFS approach also requires rigid body modes of the TS substructure if in free-floating conditions. Computing rigid body modes from measurements is possible but challenging, therefore a numerical or analytical model of the TS is often required. The modal identification step assures the MCFS reduction bases, although extracted from the measurements, to be relatively noise-free. For the same reason, modal reduction bases may be useful in experimental decoupling applications.

[19] More information on CMS limitations for this specific study is provided in Appendix B.

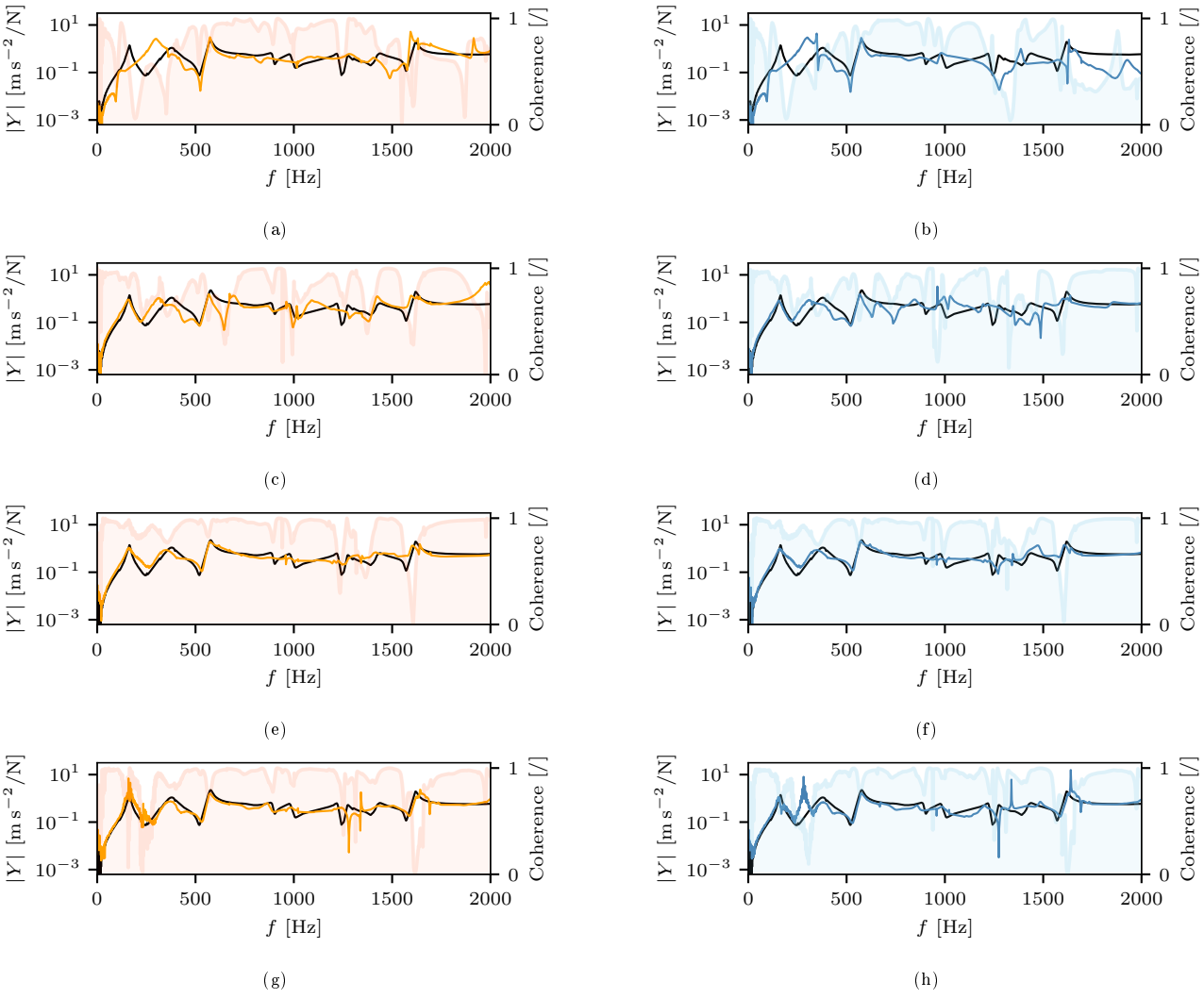

Figure 17: Amplitude and coherence of a FRF of $\mathbf{Y}^{\mathrm{AB}}$ using MCFS and SVT approach with various number of mode shapes/singular modes retained in the reduction bases; a) first 6 mode shapes, b) first 6 singular modes, c) first 8 mode shapes, d) first 8 singular modes, e) first 10 mode shapes, f) first 10 singular modes, g) first 12 mode shapes, h) first 12 singular modes. (reference, TS approach, SVT approach, coherence on TS approach, coherence on SVT approach)

So far, no criteria are available to motivate the proper selection of interface DoFs for the MCFS approach. The selection thus depends solely on the judgment of the experimentalist.

On the other hand, SVT requires no numerical or geometrical model of the structure as the reduction bases are extracted directly from the measurements. The simplicity of the SVT is evident in this aspect. Furthermore, the selection of DoFs retained in the reduction for SVT can be led by observing corresponding frequency-dependent singular values of the TS admittance matrix. This might only be problematic in certain frequency bands, where, for instance, noise and poorly controlled or observed dynamics is predominant.

Both MCFS and SVT approaches offers significant flexibility when defining reduction bases (although this has not been investigated in the scope of this paper, but has already been suggested in [17]). For instance, physical/singular modes of BTS and A can be used to define the reduction bases. Available datasets can also be concatenated and then processed by the SVD, which may provide more relevant reduced subspaces for assembled configuration, as suggested in [16].

Both MCFS and SVT can predict accurate assembly response, yet require additional measurement effort due to the presence of the TS substructure. A study using an equivalent numerical model of the TS substructure in the coupling workflow instead of experimental one demonstrated this effort can be effectively reduced and that the higher number of modes may improve response predictions in various frequency bands. The use of a numerical TS also eliminates the need for a modal identification step, which is particularly advantageous since no user-selection is required to obtain the modes. However, the TS substructure still needs to be manufactured to be incorporated into the coupling workflow and its numerical counterpart carefully modelled and preferably updated to correlate with the measured response model.

VPT as a geometric reduction also requires knowledge of the system geometry to define reduction bases. Furthermore, the VPT approach significantly reduces measurement effort (no TS substructure required, inputs and outputs on A and B do not need to be collocated). Although the measurement benefits of VPT are clear, its prediction accuracy cannot match the MCFS and SVT approaches. The proper selection of interface DoFs depends solely on the judgment of the experimentalist, which proved to be problematic for the VPT approach in this study. Within this experimental study, a rigid connection between the substructures was assumed for the VPT approach. Given that this assumption is not valid, joint effects can be treated as described in [1].

If poor conditioning of the interface flexibility matrix is observed, regularization techniques are suggested to prevent error amplification in the predicted response.

6. Conclusions

In this work, the coupling of continuous interfaces within frequency based substructuring is investigated. Three different approaches are studied that differ in the choice of the reduction bases to mitigate measurement errors and redundant dynamic interface behaviour. The MCFS method exploits flexible fixture's physical mode shapes for measured output and input DoFs, identified in a single step using multi-reference modal identification, as a reduction bases. SVT builds reduction bases from dominant singular vectors extracted directly from the available fixture's FRF dataset. VPT is presented in the form of multiple VPs approximating flexible interface motion by piece-wise rigid interface regions.

The MCFS and SVT methods offer similar and fairly consistent prediction of the coupled response throughout the entire frequency range of interest. The drawback of the methods is the requirement to use an additional flexible fixture (transmission simulator) in the coupling workflow. This step is necessary to get a common reduction bases, however it introduces additional measurement effort in the coupling process. VPT with its geometrical reduction bases avoids the collocation requirement of the measured DoFs and thus significantly reduces the measurement effort. The difficulties of the VPT are attributed to the interface DoFs selection which can quickly lead to poor conditioning of the interface flexibility matrix and inaccurate response prediction of the assembly. The presented results further motivate the need to estimate frequency dependent reduction bases for all three approaches.

The reviewed methods are implemented in the open-source *python* package *pyFBS*, thus the comparison is fully reproducible using the package documentation.

Acknowledgements

The authors D. Ocepek, G. Čepon and M. Boltežar acknowledge partial financial support from the core research funding P2-0263 and the applied research project L2-1837, both financed by ARRS, the Slovenian research agency.

Appendix A. Weakening using output and input modes

Let us assume that $\mathbf{Y}_{oi}$ can be exactly expressed by $\mathbf{\Phi}_o$ and $\mathbf{\Phi}_i$ using mode superposition. For the sake of simplicity, damping is neglected. Then, the projection into the reduced subspace can be written as:

$$\mathbf{Y}_{\text{weak}} = \mathbf{\Phi}_{o,m}^{+}\,\mathbf{Y}\,\left(\mathbf{\Phi}_{i,m}^{+}\right)^{\text{T}} \equiv \mathbf{\Phi}_{o,m}^{+}\,\frac{\mathbf{\Phi}_o\,\mathbf{\Phi}_i^{\text{T}}}{\omega^2\,\mathbf{I}-\boldsymbol{\omega}_r^2}\,\left(\mathbf{\Phi}_{i,m}^{+}\right)^{\text{T}} = \frac{\mathbf{\Phi}_{o,m}^{+}\,\mathbf{\Phi}_o\,\left(\mathbf{\Phi}_{i,m}^{+}\,\mathbf{\Phi}_i\right)^{\text{T}}}{\omega^2\,\mathbf{I}-\boldsymbol{\omega}_r^2} = \frac{\mathbf{\Phi}_{o,\text{weak}}\,\mathbf{\Phi}_{i,\text{weak}}^{\text{T}}}{\omega^2\,\mathbf{I}-\boldsymbol{\omega}_r^2}. \quad \text{(A.1)}$$

Relation above shows that the admittance matrix in the reduced domain ($\mathbf{Y}_{\text{weak}}$) can be expressed using mode superposition from output/input modes projected in the subspace composed by a truncated set of m output/input modes ($\mathbf{\Phi}^{+}_{o,m}\,\mathbf{\Phi}_o$ and $\mathbf{\Phi}^{+}_{i,m}\,\mathbf{\Phi}_i$, respectively).

Appendix B. Mode complexity and CMS

In cases where one or more substructures are highly or non-proportionally damped, using FBS to perform the assembly is preferred. The use of CMS for such cases is hardly feasible, as elaborated for our case study in the following.

Inspecting a stabilization plot as a result of a multi-reference modal identification reveals high modal density for substructure A in the frequency range of interest (Fig. B.18). Furthermore, poles are not sufficiently stable and it is thus challenging to select physically meaningful poles. For the same reason, the use of so-called 'modal filtering' using the superposition of selected modes for FRF reconstruction is not advisable for this case study.

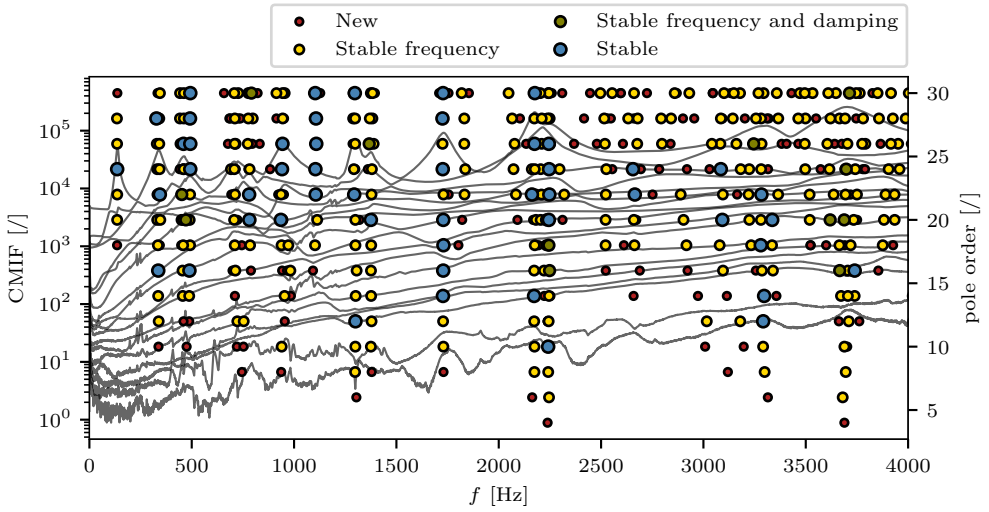

Figure B.18: Stabilization plot for modal parameter identification of substructure A.

CMS assumes the mode shape matrix for each substructure to be mass-normalized, i.e. scaled in such a way that the modal mass matrix is identity, thereby restricting it to be real-valued. In this study, Modal Complexity Factor (MCF) [23] was used to assess if identified modes can be treated as real. MCF can be seen as an indicator, bonded between 0 and 1, where values closer to one indicate that the mode is real-valued. MCF was applied to estimate the complexity of the first flexible A-normalized mode (i.e. scaled in such a way matrix $\mathbf{A}$ in state-space analysis is identity [24]) identified using multi-reference modal identification [21] for substructures BTS, TS and A. In Fig. B.19, MCF values are accompanied by a visual depiction of complexity by plotting the corresponding A-normalized mode shapes into a complex plane. It is evident that the modes for lightly damped BTS and TS are real as its components tend to form a straight line, while mode of highly damped substructure A is clearly complex (shows significant dispersion in the complex plane) and cannot be mass-normalized.

On the other hand, the design and modelling of the TS structure is always left to the experimentalist. Hence designing and manufacturing a lightly damped structure with well separated modes is always possible. Modal identification on such structures is straightforward and modes for input and output DoFs used in transformation matrices $\mathbf{T}_{\text{u}}$ and $\mathbf{T}_{\text{f}}$ in Eq. (11) can be obtained with ease (or even from the numerical model of the TS).

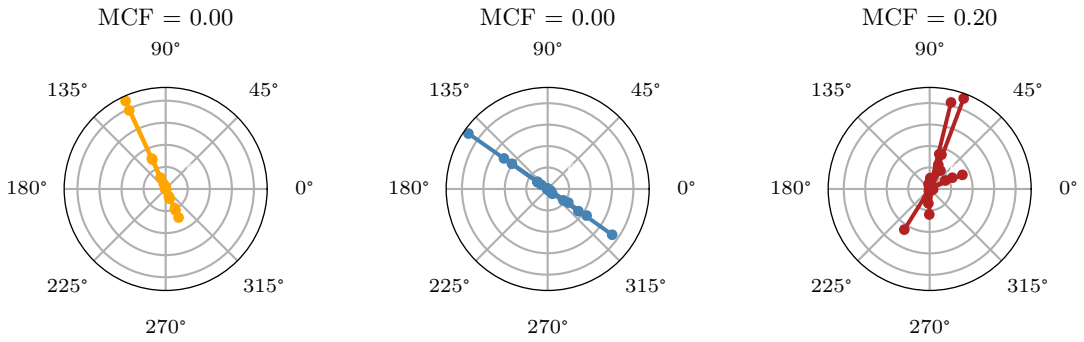

Figure B.19: Complexity of the identified mode shapes; a) substructure BTS, b) substructure TS, c) substructure A.

References

[1] M. S. Allen, D. Rixen, M. Van der Seijs, P. Tiso, T. Abrahamsson, R. L. Mayes, Substructuring in Engineering Dynamics: Emerging Numerical and Experimental Techniques, Vol. 594, Springer, 2019.

[2] D. de Klerk, D. J. Rixen, S. Voormeeren, General framework for dynamic substructuring: history, review and classification of techniques, AIAA journal 46 (5) (2008) 1169–1181.

[3] D. de Klerk, D. J. Rixen, S. Voormeeren, P. Pasteuning, Solving the rdof problem in experimental dynamic sybstructuring, in: International modal analysis conference IMAC-XXVI, 2008, pp. 1–9.

[4] S. Voormeeren, D. De Klerk, D. Rixen, Uncertainty quantification in experimental frequency based substructuring, Mechanical Systems and Signal Processing 24 (1) (2010) 106–118.

[5] J. Meggitt, A. Moorhouse, A covariance based framework for the propagation of correlated uncertainty in frequency based dynamic sub-structuring, Mechanical Systems and Signal Processing 136 (2020) 106505.

[6] F. Trainotti, M. Haeussler, D. Rixen, A practical handling of measurement uncertainties in frequency based substructuring, Mechanical Systems and Signal Processing 144 (2020) 106846.

[7] M. V. van der Seijs, D. D. van den Bosch, D. J. Rixen, D. de Klerk, An improved methodology for the virtual point transformation of measured frequency response functions in dynamic substructuring, in: 4th ECCOMAS thematic conference on computational methods in structural dynamics and earthquake engineering, Vol. 4, 2013.

[8] M. V. van der Seijs, Experimental dynamic substructuring: Analysis and design strategies for vehicle development, Ph.D. thesis, Delft University of Technology (2016).

[9] E. Pasma, M. v. d. Seijs, S. Klaassen, M. v. d. Kooij, Frequency based substructuring with the virtual point transformation, flexible interface modes and a transmission simulator, in: Dynamics of Coupled Structures, Volume 4: Proceedings of the 36th IMAC, A Conference and Exposition on Structural Dynamics 2018, Springer, 2018, pp. 205–213.

[10] J. O. Almirón, F. Bianciardi, W. Desmet, Flexible interface models for force/displacement field reconstruction applications, Journal of Sound and Vibration 534 (2022) 117001.

[11] G. Čepon, D. Ocepek, J. Korbar, T. Bregar, M. Boltežar, Sensitivity-based characterization of the bias errors in frequency based substructuring, Mechanical Systems and Signal Processing 170 (2022) 108800.

[12] T. Bregar, N. Holeček, G. Čepon, D. J. Rixen, M. Boltežar, Including directly measured rotations in the virtual point transformation, Mechanical Systems and Signal Processing 141 (2020) 106440.

[13] M. S. Allen, R. L. Mayes, E. J. Bergman, Experimental modal substructuring to couple and uncouple substructures with flexible fixtures and multi-point connections, Journal of Sound and Vibration 329 (23) (2010) 4891–4906.

[14] D. Roettgen, B. Seeger, W. C. Tai, S. Baek, T. Dossogne, M. Allen, R. Kuether, M. R. Brake, R. Mayes, A comparison of reduced order modeling techniques used in dynamic substructuring, in: Dynamics of Coupled Structures, Volume 4: Proceedings of the 34th IMAC, A Conference and Exposition on Structural Dynamics 2016, Springer, 2016, pp. 511–528.

[15] R. L. Mayes, Tutorial on experimental dynamic substructuring using the transmission simulator method, in: Topics in Experimental Dynamics Substructuring and Wind Turbine Dynamics, Volume 2: Proceedings of the 30th IMAC, A Conference on Structural Dynamics, 2012, Springer, 2012, pp. 1–9.

[16] M. Pogačar, G. Čepon, M. Boltežar, Weakening of the multi-point constraints in modal substructuring using singular value decomposition, Mechanical Systems and Signal Processing 163 (2022) 108109.

[17] F. Trainotti, T. Bregar, S. Klaassen, D. Rixen, Experimental decoupling of substructures by singular vector transformation, Mechanical Systems and Signal Processing 163 (2022) 108092.

[18] G. Strang, Computational science and engineering, Vol. 791, Wellesley-Cambridge Press Wellesley, 2007.

[19] R. Allemang, D. Brown, A complete review of the complex mode indicator function (cmif) with applications, in: Proceedings of ISMA International Conference on Noise and Vibration Engineering, Katholieke Universiteit Leuven, Belgium, 2006, pp. 3209–3246.

[20] T. Bregar, A. El Mahmoudi, M. Kodrič, D. Ocepek, F. Trainotti, M. Pogačar, M. Göldeli, G. Čepon, M. Boltežar, D. J. Rixen, pyfbs: A python package for frequency based substructuring, Journal of Open Source Software 7 (69) (2022) 3399.
[21] P. Guillaume, P. Verboven, S. Vanlanduit, H. Van Der Auweraer, B. Peeters, A poly-reference implementation of the least-squares complex frequency-domain estimator, in: Proceedings of IMAC, Vol. 21, A Conference & Exposition on Structural Dynamics, Society for Experimental Mechanics, 2003, pp. 183–192.
[22] T. Gialamas, D. Tsahalis, D. Otte, H. Van der Auwaraer, D. Manolas, Substructuring technique: improvement by means of singular value decomposition (svd), Applied Acoustics 62 (10) (2001) 1211–1219.
[23] S. Greś, M. Döhler, P. Andersen, L. Mevel, Uncertainty quantification for the modal phase collinearity of complex mode shapes, Mechanical Systems and Signal Processing 152 (2021) 107436.
[24] R. Lin, J. Zhu, On the relationship between viscous and hysteretic damping models and the importance of correct interpretation for system identification, Journal of Sound and Vibration 325 (1-2) (2009) 14–33.